Vibration Analysis of Twin-Screw Compressors Under Partial Load Design: A Case Study

Leila BAKHTIARYFARD[1], Shi-Xian CHEN[1], Yu-Ren WU[1]*, Sheng-Hung HSIEH[2], Yu-Hua HUANG[2]

[1]National Central University, Department of Mechanical Engineering,
Zhongli, Taiwan, R.O.C.
E-mail: yurenwu@ncu.edu.tw

[2]Hanbell Precise Machinery Co., Ltd.,
Taoyuan, Taiwan, R.O.C.
E-mail: Shhsieh@hanbell.com

* Corresponding Author

ABSTRACT

In the practical operation, twin-screw refrigerant compressors may suffer the partial load for a longer period than the full load, while different working condition leads to different response of noise and vibration on the compressor. In this paper, a new approach has been proposed to assess the vibration of a twin-screw refrigeration compressor under 25%, 50%, 75% and 100% load conditions. A powerful computational fluid dynamic (CFD) software, CFX, coupled with a professional grids generation software, TwinMesh, has been used to simulate the rotor loads and p-V indicator diagram which are then checked by the compressor manufacturer's machine type selection program. Next, the gas-induced loads are applied in a rotor-bearing system established based on the multi-body dynamics for the purpose to assess the vibration signal and give some conclusions for different signal features.

1. INTRODUCTION

A twin screw compressor is a positive displacement rotary machine consisting of a pair of meshing helical rotors, contained in a casing, which together form a varying working chamber in operation. Nowadays, screw machines are widely used in industrial plants and processes due to their compact structure, high efficiency and good adaptability to different refrigeration and air-conditioning systems (Stosic *et al.*, 2002). For higher pressure ratios between pressure and suction side, oil is used as sealing and lubricating fluid (Spille-Kohoff *et al.*, 2015). Regardless of the type, compressors are selected for full-load design operation, which is commonly defined as the condition of maximum required capacity and pressure rise. Most of the time, however, compressors will run at operating conditions, the sliding valve mechanism is capable of controlling the screw compressor for part load operation as well. These off-design conditions may result in noise and vibration in the system which can greatly influence the operation lifetime of the rotary components of the machine. The studies so far have mostly focused on improving the efficiency and reliability of the twin-screw compressor solely on full-load design, while experience has shown noise and vibration strongly correlated to the part-load operating condition. In this regard, much effort has been done on optimization of rotor profile and thermal/structural analysis of the system using finite element analysis (Wu and Fong, 2009). Simulation technique has played an effective role in speeding up the development process of screw compressors. This paper presents one such example of an application. Using this technique, however, in the modeling of other machineries i.e., turbo compressors might look ordinary but for screw compressors this is not the case. Some of the few and most recent cases that report the modeling of screw compressors can be found in (Kennedy *et al.*, 2017). Yet, the CFD analysis of screw compressors considering part-load conditions is vague in the past studies. The reason is due to the complex nature of the screw profile that must be simulated and the very small gaps/clearances in these machines that must be modelled.

As reported in the literatures, Kovacevic *et al.* (2002) established a full 3-D simulation in order to determine how pressure and temperature changes inside working chamber influences compressor performance. It was concluded

that, a high-pressure rise has adverse effects but a high temperature rise may lead to an increase in delivered flow and efficiency. Stosic *et al.* (2006) checked the influence of discharge port design on mechanical noise created when rotors contact. They found out that a small adjustment of torque and pressure distribution inside working chamber can greatly effect on vibration of the system. Trial and error changes were made to the discharge port size and shape until the best result was achieved. Wang *et al.* (2012) investigated the noise and vibration of a twin screw compressor running under different loading capacity conditions experimentally. It was found out that the overall A-weighted SPL of the compressor increases with the loading capacity. The noise and vibration spectra also shown strongly correlated, especially for the peaks at some harmonics with respect to the coincident male and female screw shafts speed frequency.

Wu *et al.* (2018) proposed using a pressure pulsation dampener (PPD) in the discharge chamber of a twin screw refrigeration compressor in order to reduce the amplitude of pressure pulsation. A mathematical model was developed to design an optimal PPD. The designed model of the PPD and an experimental set-up were then developed to evaluate the effect of parameters such as oil flow rate and cavity volume on attenuation performance of the PPD. The accuracy of the model was checked by simulation results which showed a good agreement with the experimental data.

Looking up to the past literatures shows that unlike efficiency and reliability analysis of twin screw compressors there are few published references on the vibration and noise diagnosis of twin-screw compressors. This becomes critical particularly where quiet operations are required. Although, in practical cases of diagnosis of structural vibration on this type of compressors, Fujiwara *et al.* (2011), Wu and Tran (2016) did some studies, none of the authors considered the effects of part-load in their model. Therefore, the purpose of this work is to find correlation of key parameters with part-load by assessing the vibration signals established based on the multi-body dynamics analysis techniques of the rotor-bearing system.

2. CFD MODELING AND SIMULATION METHOD

The study used an oil-less 5/6 screw refrigeration compressor model RC2-410 made by Hanbell Co. in Taiwan. The male rotor has five lobes and the female rotor has six lobes with patented profiles. The built-in volume index Vi of the compressor is 3.5. The compressor is driven by a 67.9 kW motor with a variable frequency drive for speed control. Other design parameters and boundary conditions are listed in Table 1. The compressor individually is modelled and analyzed under 25%, 50%, 75% and 100% load conditions. The simulation has performed for four full rotations until the flow and pressure pulsations showed cyclic repetitions.

Table 1: Design parameters and boundary conditions

Design Parameters and Operating Conditions	Values
Outer diameter of the male rotor	87.0 mm
Outer diameter of the female rotor	70.0 mm
Length of the rotors	162.04 mm
Rotation speed (male rotor)	3000 rpm
Inlet pressure	3.58 bar
Outlet pressure	9.64 bar
Inlet temperature	283.15 K

2.1 Numerical Simulation Method and Procedure

The numerical simulation is carried out by taking the advantage of fluid flow analysis function of ANSYS WORKBENCH. In this approach, the static grids were generated with ANSYS meshing while the rotating and deforming ones resulted from a customized grid generator, TwinMesh, from CFX-Berlin. At the beginning, the fluid domain is extracted from solid domain using SpaceClaim. The extracted geometry then is exported to ANSYS mesh for the purpose of static grids generation and defining interfaces and boundaries. The interfaces and boundaries are defined to the CFD solver using “Named Selection” function of ANSYS WORKBENCH. The same method is applied on all cases, the only difference was the definition of boundaries in radial discharge port and suction port where the by-pass channel connects suction to working chamber. Taking example of 25% loading condition radial in discharge port does not exist, however another radial interface can be seen in the connection of by-pass channel and rotors (Figure 1). The set of generated grids from rotary domain and static domain are eventually coupled with a

CFD solver. The setup created by TwinMesh provides a ready-to-use simulation setup with a little adjustment in setting parameters. The Total Energy option is checked for heat transfer and air ideal gas is used for the fluid material since the flow is compressible and for the mesh motion, the Junction Box Routine is used. The male and female rotors are given the appropriate rotational speeds and directions. Heat transfer within the solid rotors are not accounted for this simulation. User routines for the rotor movement and definition of the fluid-fluid interfaces are carried out automatically upon mesh export. CFX calculates the pressure variation in the discharge port and induced gas load as well as resultant torques imposed on screw rotors. Finally, the data obtained from simulation are coupled with ADAMS software in order to evaluate vibration under various operating conditions.

Figure 1 shows the CFD model that consists of the combination of suction port, discharge port and rotary domain (working chamber). Both the ports have an extended part to provide boundary pressure conditions. The working chamber domain itself is a deforming grid, generated using the procedure described above. The mesh quality for rotor domain is considered to be same for all of the analyzed cases. The model mesh statistics is presented in Table 2 along with the cell quality report. The rotor domain had the minimum orthogonality factor but it was below value of 10 in less than 1% of cells. Aspect ratio for rotors domain was in good control due to the fewer divisions in the radial direction and using hex elements. However, due to complication of the geometry of stator domain aspect ratio was not located in an acceptable range for some of the cells.

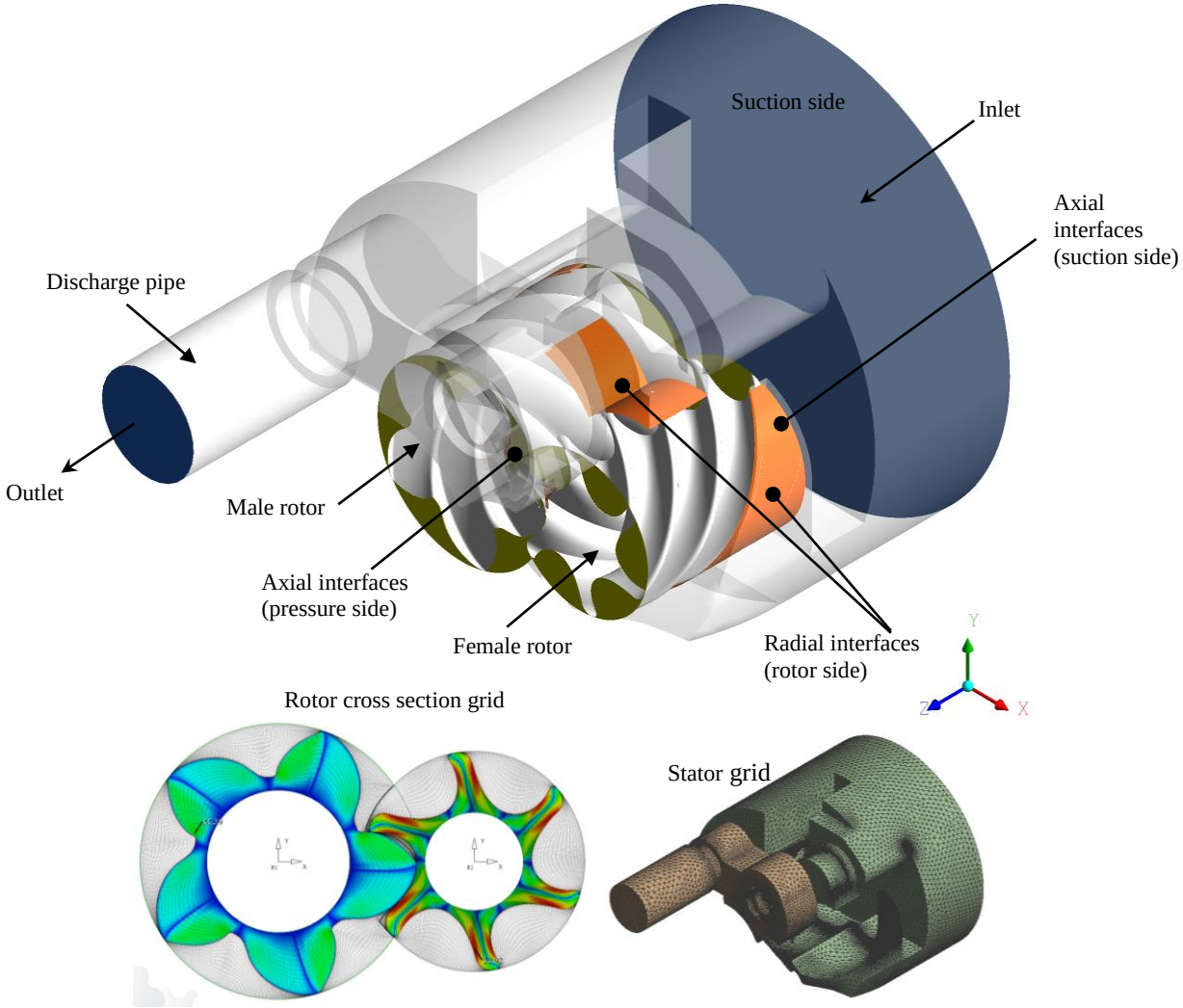

Figure 1: CFD model with the different regions and boundaries along with generated mesh at 25% load

Table 2: Mesh statistics and cell quality report for case 1

Fluid Domain	Cell Structure	Node Count	Cell Count	Orthogonality Angle (Min)	Aspect Ratio
Working Chambers	Hexahedral	4523814	4207800	13.7	1798
Suction Port	Tetra	158252	771771	0.22	1.16
Discharge Port	Tetra	59580	304314	0.22	1.16

3. RESULTS AND DISCUSSIONS

Numerical simulation is carried out for each of the specific aforementioned designs individually. Though, not all of the analyzed results for different operating conditions are illustrated here. Rather cases under 100% and 25% loads, are selected as example to show the fluid flow behavior change inside the working chamber. The corresponding results in the last one revolution are obtained through post-processing technology of ANSYS CFX and the selected one are plotted in Figure 2 ~ Figure 4. In order to prove the usefulness and accuracy of the simulation results, they are checked by the compressor manufacturer's machine type selection program. A good agreement between the two ways of measurements has been found.

3.1 Calculation of Pressure Variation Inside Working Chamber

Figure 2 demonstrates chamber pressure over rotation angle of male rotor for all four design loads. The pressure variation graph shows a sharper and smoother change in pressure as the part-load increases. The area under the curves is reducing which also can lead to less power consumption of the machine. More fluctuation is observed at the top of the pressure graph in the case of 50% and 25% load designs. As it is seen, the time for achieving target outlet pressure 9.64 bar has shortened significantly which can end to noise and vibration in the system as well. This can be described by, the sound pressure levels dependency to the total mechanical energy that is transformed into acoustical energy in a fraction of time. In the case of part-load designs since energy transformation occurs in a shorter time therefore higher sound level are expected. Aside from simulation, observations of the machine working in the field condition and under part-load operations confirm this issue. The boundaries pressure and temperature for all models are taken the same in order to check fluid behavior inside the working chamber under various loading conditions.

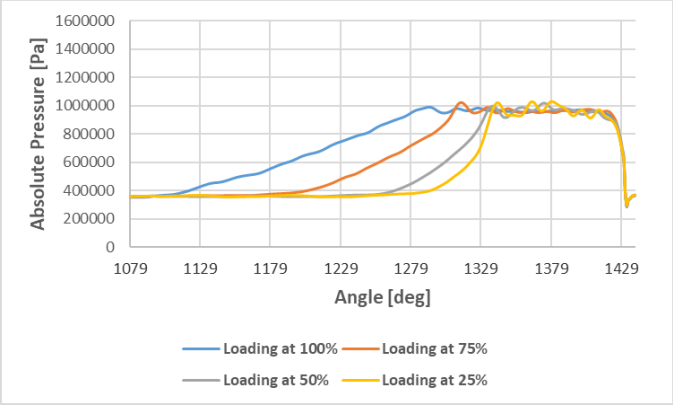

Figure 2: Chamber pressure variation over rotation angle of male rotor

3.2 Calculation of the Induced Torque and Forces on Male and Female Rotors

Based on the obtained data, following graphs are plotted. Figure 3 and Figure 4 presents the cyclic variations of the gas-induced torque and normal forces on screw rotors wall when the rotation angle of the male rotor varies. The calculated results are later used as boundary condition for the MBD model in MSC ADAMS software for doing multibody dynamic analysis. It can be seen, in Figure 3, the system torque graph suffers from more fluctuation with

a higher amplitude comparing to full-load design. A method to estimate the fluctuation of the graph is given in Equation (1). Where λ and T stand for unevenness ratio and torque, respectively. The numerical assessment results confirmed greater variation in the magnitude of system torque in the case of part-load designs, thus, larger noise and vibration are expected to be produced by the system. Aside from, imposed gas torque on male rotor and total torque graphs are almost overlapped in part-load designs particularly at 25% loading condition which can lead to structural vibration and noise in the entire system. On the other hand, calculated torque on female rotor fluctuates between positive (+) and negative (-) values which itself alone can be another source of noise in the screw rotors. The rise in system torque, eventually becomes stable with a descending running average of 155 N.m, 106 N.m, 69 N.m, and 57.3 N.m at 100% ~ 25% loading ratio, respectively.

$$\lambda = \frac{T_{max} - T_{min}}{0.5 \times (T_{max} + T_{min})} \tag{1}$$

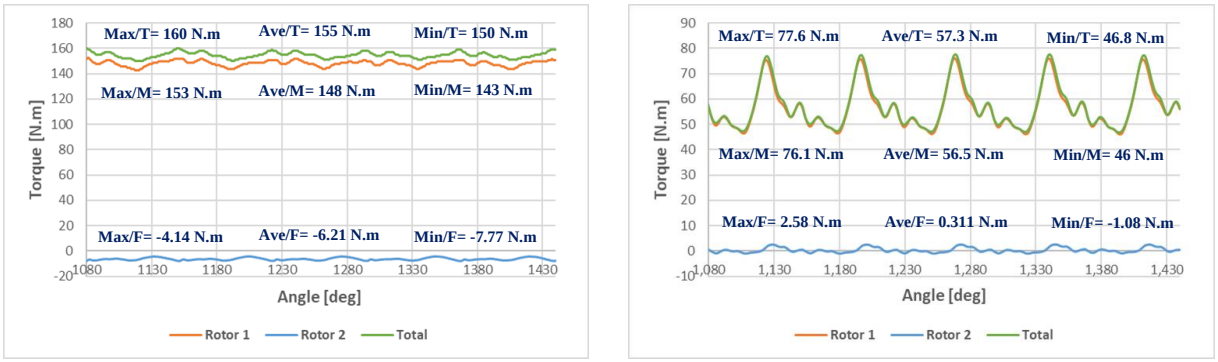

(a) (b)

Figure 3: Gas-induced torques over rotation angle; (a) Loading at 100%; (b) Loading at 25%

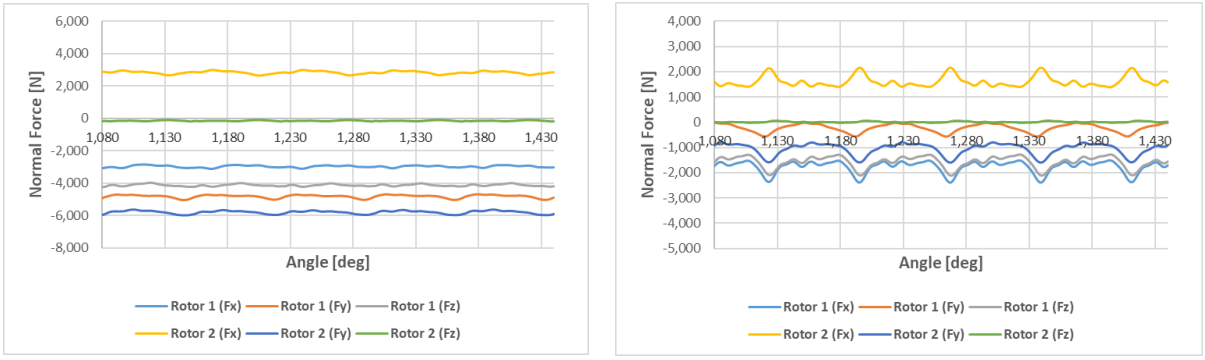

(a) (b)

Figure 4: Gas-induced forces on rotors wall over rotation angle; (a) Loading at 100%; (b) Loading at 25%

4. MBD (MULTI BODY DYNAMICS) ANALYSIS METHOD

The rotors are assembled at a practical center distance of 123.03 mm and all of the components of the MBD model are assumed to be rigid bodies. The data for the MBD simulation are given in Tables 3 and calculated in section 3.2. Two different simulation cases are analyzed and compared in vibrational point of view. Figure 6 ~ Figure 9 present the MBD-simulated contact force for the rotors, axial imposed force on bearings, and frequency spectra for the vibration signals when gas-induced cyclic loads are applied to the rotors wall. The calculated torque and induced force data in the previous section are applied as boundary conditions for further analysis in this section. The proposed MBD Model for a screw rotor and bearing system simulated using the multibody dynamics software, MSC.ADAMS is demonstrated in Figure 5. The dynamic simulations used the integrator WSTIFF and the Stabilized Index-2 (SI2) formulation (MSC ADAMS, 2017). The male rotor rotated at 3000 rpm, and the end time for the

simulation process was 0.08 second, with 50,000 time steps. The discrete data for the gas-induced cyclic forces and the torque values were imported into ADAMS as spline curves and applied to the male and female rotors using the built-in function, "AKISPL". The relevant contact settings and the material properties of steel are listed in Table 3. The contact stiffness of the rotors (K_{12}) was determined using Hertz contact theory for circular contact given in Equation (2):

$$K = 2E_s\left(\frac{3F_n\rho_s}{4E_s}\right)^{1/3} \tag{2}$$

Where, $E_s=E_1.E_2/(E_1+E_2)(1-\nu^2)$ is the synthetic elastic modulus, E_1 and E_2 are the elastic modulus of the two contact bodies and ν is Poisson's ratio, $\rho_s=\rho_1.\ \rho_2/(\rho_1+\rho_2)$ is the synthetic radius of curvature, ρ_1 and ρ_2 are the radius of curvature for the two contact bodies at the contact point (Wu and Tran, 2016).

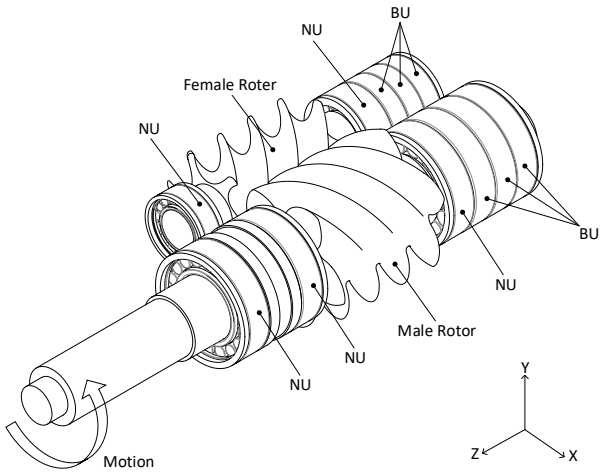

Figure 5: 3-D MSC ADAMS model of the screw-rotor and bearing system

Table 3: Simulation parameters and material properties

Contact Settings	Values	Material Properties	Values
Contact Stiffness of the Rotors (K_{12})	2.42×10^5 ($N.\ mm^{-1}$)	**Density**	7.80×10^{-6} (kg/mm^3)
Stiffness for other Contact Pairs (K_o)	1.0×10^5 ($N.\ mm^{-1}$)	**Elastic Modulus**	2.07×10^5 ($N.\ mm^{-2}$)
Force Exponent (e)	2.2	**Poisson's Ratio**	0.29
Damping Coefficient of the Rotors (C_{12})	10 ($N.s.\ mm^{-1}$)	**Coefficient of Static Friction**	0.23
Damping Coefficient for other Contact Pairs (C_o)	10 ($N.s.\ mm^{-1}$)	**Coefficient of Kinetic Friction**	0.16
Penetration Depth (d_s)	0.1 *mm*	-	-

4.1 Simulation of the Contact Forces between Rotors

In this case, the gas-induced cyclic loads are applied to the rotor surfaces. The input data for the MBD simulation are given in Tables 3 and section 3.2. The MBD simulated contact force for two of operating conditions are plotted in Figure 6. It is seen that the average contact force decreases from 8132.7044 N to 2274 N, which corresponds to the scenarios whereby compressor is working at 100% and 25% loading condition (72.04%↓). Aside from, the three-dimensional waterfall plot of the frequency spectra of the vibration signals are obtained through MBD simulation are shown in Figure 7. The theoretical base rotation frequency for the male rotor is 50 Hz (=3000 rpm/60 sec), the theoretical base meshing frequency is 250 Hz (=5 teeth × 50 Hz), and its harmonic frequencies can be evaluated in

advance. In order to check the accuracy of the simulation results, they are compared with results in the existing literature similar to this study (Wu and Tran, 2016). For example, for the case of compressor loading at 100%, results in Figure 6(a) (=8132.7044 N) and in Figure 18 (Wu and Tran, 2016) (=6118.1N) are compared. Theoretically, by increasing rotation speed from 3000 rpm to 3600 rpm, it is expected change in contact force (F_t) with 1.2 ratio. Numerical assessment ratio of the average calculated contact force in MBD simulation confirms the correctness of this results. The simulated components of the frequency spectra for the first five peak are listed and compared in Table 4. The percentage difference between result obtained in the literature and current simulation can be explained by differences in the input rotation speed of 3600 rpm in (Wu and Tran, 2016).

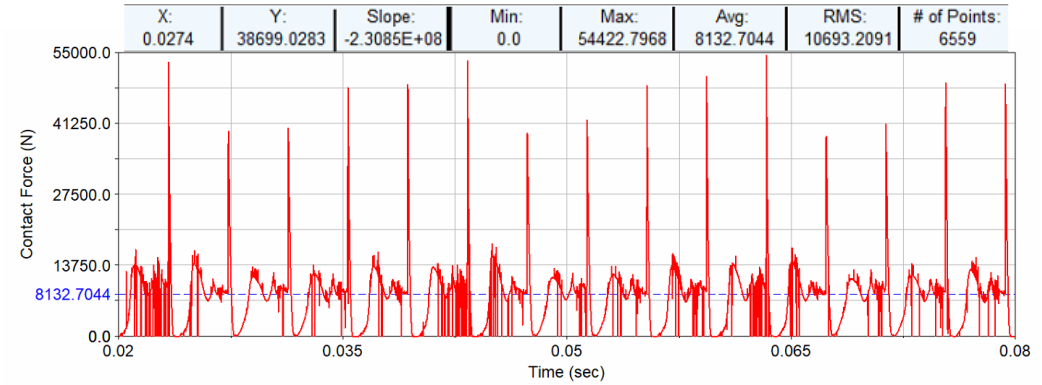

(a)

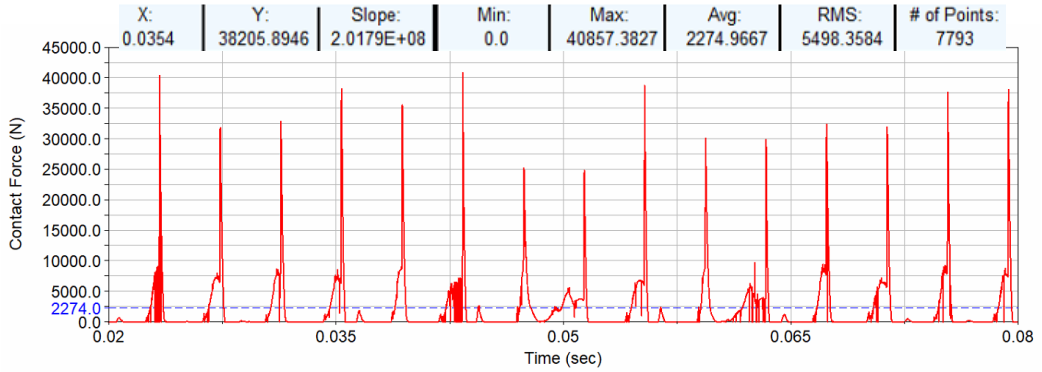

(b)

Figure 6: The MBD-simulated contact force for the rotors; (a) Loading at 100%; (b) Loading at 25%

From the following 3-D waterfall plot (Figure 7), It is found out that:

1.The overall peak amplitudes for Z component forces under different load conditions are greater than those for X and Y component forces. It is a characterastic of the positive displacement machine that the gas is compressed to higher pressure from the suction end to the discharge end.

2.At f_{m1}, the peak amplitudes of three directions under 50% load condition is higher than under other conditions.

3.Under 100% load condition, the peak amplitudes at $2f_{m1}$ are greater than those at f_{m1}.

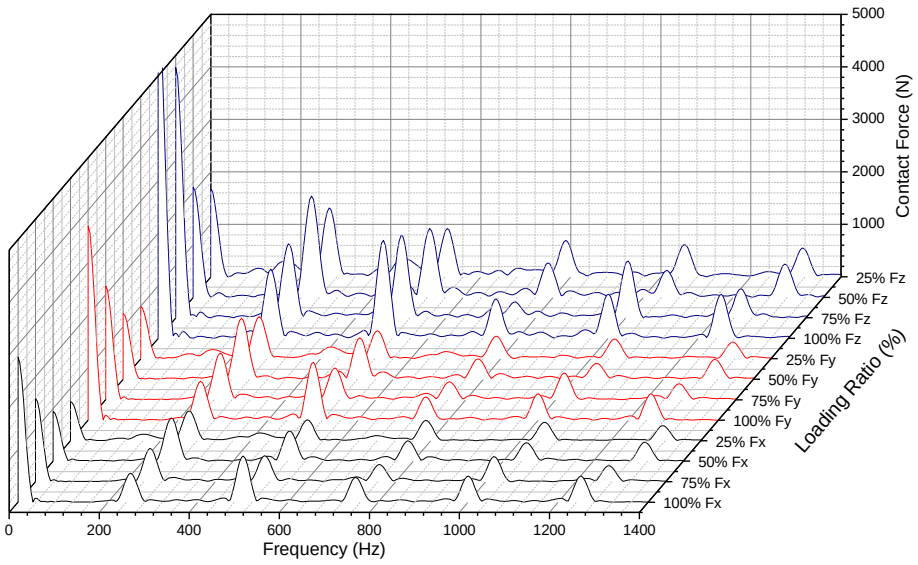

Figure 7: 3-D waterfall plot of the frequency spectra for the vibration signals loading at 25%~100%

Table 4: The simulated frequency spectra results comparison (contact force)

Frequency / Loading	f_{m1} (Hz)	$2f_{m1}$ (Hz)	$3f_{m1}$ (Hz)	$4f_{m1}$ (Hz)	$5f_{m1}$ (Hz)
Component Z of Contact Force (Hz , N)					
25%	(249.7 , 1312.5)	(499.4 , 917.7)	(749.0 , 692.3)	(998.7 , 611.2)	(1248.4 , 546.5)
50%	(249.9 , 1929.5)	(499.8 , 1307.5)	(749.7 , 654.6)	(999.6 , 513.6)	(1249.5 , 631.7)
75%	(249.8 , 1407.5)	(499.5 , 1569.0)	(749.3 , 300.5)	(999.0 , 1083.4)	(1248.8 , 557.2)
100%	(250.3 , 1317.3)	(500.5 , 1864.0)	(750.8 , 751.5)	(1001.1 , 839.6)	(1251.4 , 835.3)
Component Y of Contact Force (Hz , N)					
25%	(249.7 , 801.9)	(499.4 , 536.6)	(749.0 , 429.1)	(998.7 , 373.7)	(1248.4 , 318.0)
50%	(249.9 , 1163.4)	(499.8 , 790.1)	(749.7 , 388.3)	(999.6 , 303.5)	(1249.5 , 381.0)
75%	(249.8 , 891.8)	(499.5 , 607.3)	(749.3 , 340.2)	(999.0 , 506.4)	(1248.8 , 303.6)
100%	(250.3 , 741.2)	(500.5 , 1105.7)	(750.8 , 443.4)	(1001.1 , 503.9)	(1251.4 , 499.0)
Component X of Contact Force (Hz , N)					
25%	(249.7 , 569.4)	(499.4 , 397.4)	(749.0 , 385.7)	(998.7 , 348.3)	(1248.4 , 286.6)
50%	(249.9 , 824.6)	(499.8 , 577.8)	(749.7 , 387.1)	(999.6 , 351.6)	(1249.5 , 362.5)
75%	(249.8 , 631.9)	(499.5 , 493.8)	(749.3 , 326.0)	(999.0 , 477.0)	(1248.8 , 304.3)
100%	(250.3 , 550.8)	(500.5 , 878.9)	(750.8 , 470.6)	(1001.1 , 495.9)	(1251.4 , 469.2)

An outstanding feature of the standard screw compressor is the ability of stepless capacity control with the slide valve system. The change in loading condition resulting from the axial movement of the slide valve affects not only the performance of compressor but also the characteristics of noise and vibration as it is shown in Figure 7. In the vibration contact force spectrum, a cluster of peaks at approximately 250 Hz and 500 Hz indicates an abnormality in the compressor. And the waveform indicates that the unusual signal is generated in a series of impacts repeating at relatively low frequencies in particular at 50% loading condition. It appears that a complex change occurs in the characteristics of noise and vibration under part load operation. The accurate cause of the difference in noise and vibration cannot be confirmed now. But it can be assumed that it is resulting from the returning oil from the bearings and the mechanical seal will sometimes obstruct a stable operation of compressor under reduced gas flow. Moreover, the slide valve sometimes vibrates at the fundamental screw frequency and by impacting on the casing, it would cause an excessive noise and/or vibration problem in extreme case (Fujiwara and Sakurai,1986).

5. CONCLUSION

The material presented in this study is directed toward providing a basic understanding of the fundamental characteristics of noise and vibration in an oil-free screw compressor under partial load design. Simulation technique has played an important role in our work. The essential advantage of a numerical simulation was the visualization of the fluid flow behavior effects on the structure without needing time consuming and costly experiments. Thus, computational fluid dynamic (CFD) together with MBD (multi body dynamics) analysis has been used as an effective way to predict the compressor's dynamic response and to determine the reasons for structural vibration. A novel method to analyze the dynamics of a pair intermeshing rotors is proposed that combines the cyclic variations of the gas-induced forces and torque on the male and female rotors with the rotation angle of male rotor. From the results of these simulations it is believed that design and operating conditions both inf1uence on pressure pulsations of discharge and suction gas. More importantly, they inf1uence on dynamic induced gas forced on rotors and the mechanical contact forces between rotors. thereby control all the characteristics of noise and vibration. The following conclusions to be drawn:

(a) The contact forces obtained for the two rotors of a twin screw compressor using MBD simulation were almost in good agreement with our past study which demonstrates that the proposed simulation method for both CFD and MBD analysis are accurate.
(b) As a result of compressing gas load from lower pressure to higher pressure, the overall peak amplitudes for Z component forces under different load conditions are greater than those for X and Y component forces.
(c) Higher peak amplitudes are observed at f_{m1}, in three directions under 50% load condition than under other conditions.
(d) While, under 100% load condition, the peak amplitudes occur at $2f_{m1}$.
(e) The average value of the contact force decreases as the rotational speed of the male rotor increases.
(f) The average value of the contact force dropped for 72.04% when compressor change working condition from 100% to 25% loads.
(g) Reduction of the imposed forces on rotors and bearing system under part-load designs can greatly influence the working lifetime of the machine.

Although the proposed modeling method is proven to be effective to simulate the dynamics and to evaluate the vibration signal, the details of the performance of this new model still need to be studied. Planned future work will conduct the experimental work for all part-load designs, to practically measure the magnitude of the above calculated parameter and compare them with the results obtained from MBD simulation. Aside from, the fault recognition using FFT signal analysis and the probable solutions will be discussed in our future studies.

ACKNOWLEDGEMENT

The authors would like to thank to the official of HANBELL Precise Machinery Co., Ltd of Taiwan and MOST research fund [no. 106-2221-E-008-045] for their financial support of this research.

REFERENCES

Stosic N., Smith I. K., Kovacevic A., (2002). A Twin Screw Combined Compressor and Expander for CO_2 Refrigeration Systems. Proc. Int. Compressor Conf. at Purdue, Paper 1591.

Spille-Kohoff A., Hesse J., Shorbagy A. E., (2015). CFD Simulation of a Screw Compressor Including Leakage Flows and Rotor Heating. IOP Conference Series: Materials Science and Engineering; 90; 1-11; Int. Conf. on Compressors and Their Systems, London, UK.

Wu Y.R., Fong Z.H., (2009). Optimization Design of an Explicitly Defined Rack for the Generation of Rotors for Twin-screw Compressors. Mechanism and Machine Theory, vol. 44 (1), pp.66–82.

Kennedy S., Wilson M., Rane S., (2017). Numerical Analysis of an Oil-free Twin Screw Compressor Using 3D CFD and 1D Multi-Chamber Thermodynamic Model. IOP Conference Series: Materials Science and Engineering; 232; 1-10; Int. Conf. on Compressors and Their Systems, London, UK.

Kovacevic A., Stosic N., Smith I.K., (2002). The Influence of Rotor Deflection upon Screw Compressor Performance. Centre for Positive Displacement Compressor Technology City University, UK.

Stosic N., Mujic E., Kovacevic A., Smith I. K., (2006). The Influence of Discharge Ports on Rotor contact in Screw Compressors. Proc. Int. Compressor Conf. at Purdue, Paper C010.

Wang B.T, Hsieh C.H, Wang W.C, Liu C.L, (2012). Noise and Vibration Characteristic Studies of Twin Screw Compressor in Different Operating Conditions. Proc. Int. Compressor Conf. at Purdue, Paper 1427.

Wu X., Xing Z., Chen W., Wang X., (2018). Performance Investigation of a Pressure Pulsation Dampener Applied in the Discharge Chamber of a Twin Screw Refrigeration Compressor. International journal of Refrigeration, vol. 85, pp. 70–84.

Fujiwara A., Matsuo K., Yamashita H., (2011). Vibration Analysis of Oil-Injected Twin-Screw Compressors Using Simple Simulated Waveforms. Proceedings of the Institution of Mechanical Engineers, Part E: Journal of Process Mechanical Engineering, vol. 225 (2), pp. 105-116.

Wu Y.R., Tran V.T, (2016). Dynamic Response Prediction of a Twin-Screw Compressor with Gas-Induced Cyclic Loads Based on Multi-Body Dynamics. International Journal of Refrigeration, vol. 65, pp. 111-128.

Fujiwara A., Sakurai N., (1986). Experimental Analysis of Screw Compressor Noise and Vibration. Proc. Int. Compressor Conf. at Purdue, Paper 553.